Improvement in Voltage, Thermal, Mechanical Stability and Ion Transport Properties in Polymer-Clay Nanocomposites

A. L. Sharma, Awalendra K. Thakur

Department of Physics and Meteorology, Indian Institute of Technology (I. I. T.), Kharagpur – 721302, India

Received 28 November 2009; accepted 16 April 2010
DOI 10.1002/app.32677
Published online 29 June 2010 in Wiley InterScience (www.interscience.wiley.com).

ABSTRACT: We report novel results on optimization of intercalated polymer-clay nanocomposite endowed with desirable properties like, (i) very high ionic conductivity ($\sim 10^{-3}$ S cm^{-1}) at room temperature, (ii) substantial improvement in voltage stability ($\sim$ 5.6 V), mechanical stability (25 MPa), and thermal stability (250°C) (iii) $t_{ion} \sim 99\%$ and cation transport number (t_{Li+}) $\sim$ 67%: Intercalation of polymer salt $(PAN)_8LiCF_3SO_3$ complex into dodecylamine modified montmorillonite clay (DMMT) nanometric channels has been confirmed by X-ray diffraction and Transmission electron microscopy analysis. Complex impedance spectroscopy suggests bulk electrical conduction in the high frequency region and electrode polarization effect at the low frequencies. The experimental value of conductivity, voltage, and mechanical stability is observed to be invariably higher in polymer nanocomposite film when compared with clay free polymer-salt complex film. The same is true for cation transport. The optimized polymer film serves dual purpose of electrolyte and separator in energy storage devices. © 2010 Wiley Periodicals, Inc. J Appl Polym Sci 118: 2743–2753, 2010

Key words: polymer nanocomposites; complex impedance spectroscopy; cation transport; voltage stability; thermal stability; energy storage device

INTRODUCTION

Dimensionally flexible ionic conductors based on polymer are considered promising candidates as the separator between electrode compartments in solid state ionic devices such as high energy density batteries, supercapacitors, PEM fuel cells, etc.[1–3] A wide variety of polymeric ionic conductors like gel polymer electrolytes (GPEs),[4] solid polymer electrolytes (SPEs),[5] composite polymer electrolytes (CPEs),[6] etc. have been studied and evaluated over a decade now. A comparison of the properties of such systems reported in literature[7–9] indicates that, it is very difficult to achieve all the desirable properties for device applications in a single material system. They are as follows: (i) ionic conductivity $\sim 10^{-3}$ S cm^{-1} under ambient conditions, (ii) voltage stability $\geq$ 3 V, (iii) adequate thermal stability within operational temperature limits, (iv) stability toward electrode at the interface, and (v) dimensional stability $\geq$3 MPa suitable for design flexibility. As a consequence the practical realization of a light weight high energy density device comprising of all solid components still remains a challenge.

Correspondence to: A. K. Thakur (akt@phy.iitkgp.ernet.in).

Journal of Applied Polymer Science, Vol. 118, 2743–2753 (2010)

The primary factors responsible for low ambient conductivity in conventional solvent free solid polymeric conductors are as follows: (a) slow ion dynamics in multiphase polymeric matrix controlled by poor mobility of polymer chains (segments) at room temperature, (b) concentration polarization because of the mobility of both cation and anions in the solid polymer matrix, and (c) high internal resistance that depend on a number of intrinsic factors viz. intrinsic friction because of polymer viscosity, ion pairing and charge immobilization, etc.

Of these, the problem of concentration polarization is one of the major cause for poor ambient conduction because of simultaneous mobility of ions of opposite nature and consequent ion pairing. It can, however, be minimized to an acceptable limit by an appropriate material fabrication procedure. A number of approaches have come invogue recently to overcome the problems mentioned above. The approach of polymer nanocomposite (PNC) formation via intercalation of polymer-salt (PS) complex into nanometric clay channels (width $\sim$ 0.56 nm) of an organomodified clay such as the montmorillonite appears to be attractive. The anionic charge on the organo clay surface having high cation exchange capacity (CEC $\sim$ 80–120 mEq/100 g) may be expected to permit the entry of only cation coordinated polymer matrix into the nanometric clay channels. In this way, an effective separation between

cations and anions of the PS complex matrix can be maintained in the intercalated nanocomposite films. This inturn stabilizes the concentration polarization by minimizing the possibility of ion pair formation and providing suitable path for cation migration through intercalated channels of the clay.

The choice of polyacrylonitrile (PAN) as the polymer host for complexation with the salt ($LiCF_3SO_3$) having bulky anion is based on the factors like, (i) the presence of electron rich group ($C \equiv \ddot{N}$) with weak π bonds, (ii) possibility of easier cation coordination with polymer backbone in a polar solvent such as N, N, dimethylformamide (DMF), Dimethyl sulfoxide (DMSO), Dimethylacetamide (DMA), Ethylene carbonate (EC), Propylene carbonate (PC), etc., (iii) appreciably high mechanical strength (250–568 Pa), and (iv) significant thermal stability up to 220°C.

This article reports the results of our investigations on a nanocomposite polymer films prepared by intercalation of PS complex into the nanometric clay galleries of organomodified montmorillonite clay. Intercalation of the PS component into clay channels have been confirmed by X-Ray diffraction (XRD) analysis and observed visually in transmission electron micrographs (TEM). Complex impedance spectroscopy (CIS) has been carried out to analyze effect of clay concentration on electrical properties. Ion transport, voltage, mechanical, and thermal stability properties of the PNC films have been studied and analyzed.

EXPERIMENTAL

Materials preparation

PNC films were prepared via a standard solution cast technique, using PAN (Aldrich M.W. 1.5×10^5) as the polymer host matrix, and appropriate lithium salt ($LiCF_3SO_3$; Aldrich (Germany)). Nanocomposite formation was carried by intercalation of PS complex into nanometric channels of the dodecylamine (DDA) modified montmorillonite clay (DMMT). Clay (SWy–2) has been procured from the Source clays repository (The clay minerals society, Purdue University (USA)) and added in different weight fraction relative to polymer host. The polymer host (PAN) and salt ($LiCF_3SO_3$) was vacuum dried at 120°C for 32 h. An appropriate stoichiometric ratio of PAN was dissolved in DMF (Merck (Germany)), and the solution was stirred for 18 h. Subsequently, a calculated amount of $LiCF_3SO_3$ was added into the PAN solution and stirred for 15 h to facilitate homogeneous mixing and complexation. The stoichiometric ratio of salt in the polymer host (PAN) matrix was maintained at an optimized ratio of ($\frac{\ddot{N}}{Li} = 8$) Next, DDA modified montmorillonite clay was added into the complex PS solution in different concentration ($0 \leq x \leq 20$; x refers to clay concentration w.r.t. PAN by weight) and stirred for 12 h. Finally, the composite solution were poured in polypropylene dishes and allowed to dry under controlled conditions. Free standing polymer films were obtained on solvent evaporation. The series of PNC films so obtained can be expressed as: $(PAN)_8LiCF_3SO_3 + x$ wt %DMMT.

Material characterization

XRD of polymer films were recorded at room temperature using a ('X'Pert PRO PANalytical diffractometer model: PW3040/60) with CuKα radiation ($\lambda = 1.5418$ Á) over a range of diffraction angle ($2^\circ \leq 2\theta \leq 40^\circ$) at a scanning rate of $2^\circ min^{-1}$. High resolution transmission electron microscopy has been performed by JEOL-JEM (model: 2100, Japan), operating at 200 kV. CIS measurements of the composite films were carried out using a computer interfaced impedance analyzer (HIOKI LCR Hi-Tester Model: 3522-50, Japan) in the frequency range from 100 mHz to 100 kHz on a sample cell configuration of the type; *SS/PNC/SS* (SS stands for stainless steel blocking electrodes and PNC for PNC films). An input a.c. signal of ~ 60 mV was applied across the cell to perform impedance measurement. Ion transport number estimation has been done using Wagner's polarization technique by separating electronic and ionic contribution to the electrical charge mobility in the sample films. Ionic transport number (t_{ion}) has been calculated using the equation

$$t_{\text{ion}} = \left(\frac{I_t - I_e}{I_t}\right) \tag{1}$$

where I_t is the total current and I_e is the residual electronic current. Cation transport number of the PNC film has been determined by the combined a.c. Impedance/d.c. polarization technique developed by Vincent and coworkers.[10] Voltage stability (electrochemical potential window) of the PNC films has been analyzed by measuring the variation of residual electronic current as a function of the applied voltage across the cell *SS/PNC/SS*. The result of I-V characteristic gave an estimate of the working (breakdown) voltage obtained from the point of intercept of the suddenly rising current on the voltage axis. Thermal stability properties of the composite films has been studied by thermogravimetric analysis (TGA) using Perkin Elmer simultaneous thermal analyzer (model: Diamond) at a scan rate of $10^\circ C\ min^{-1}$ in argon atmosphere. Mechanical properties such as the tensile strength, stress-strain diagram of the thin PNC films was measured at room temperature using Hounsfield (UK) H10KS-0547 instrument at a scan speed rate of 0.75 mm min^{-1} (strain rate of 5% of sample length). The elongation produced in the polymeric films has been monitored

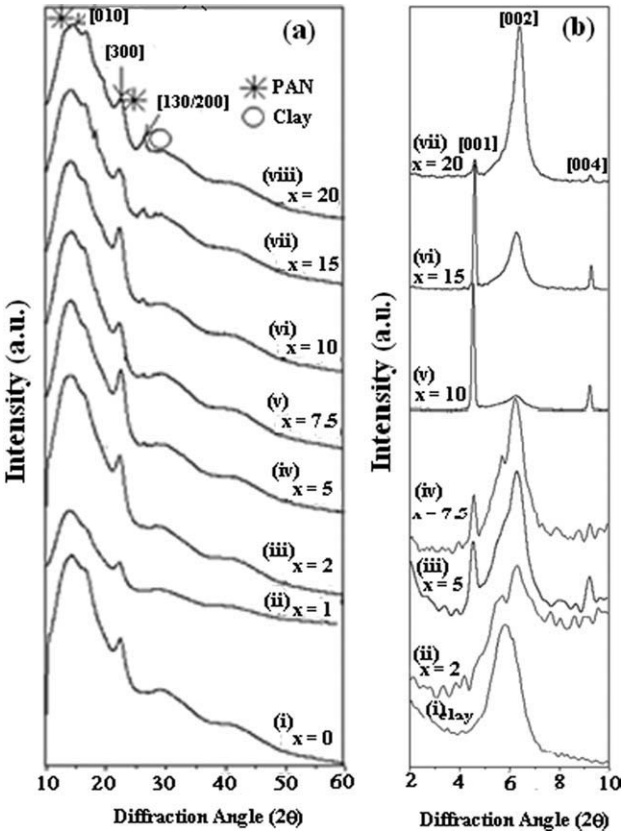

Figure 1 (a) XRD pattern of PNC films based on $(PAN)_8$-$LiCF_3SO_3$+ *x* wt % DMMT showing effect on clay concentration on polymer host peak profile; (b) Small angle XRD pattern showing evidence of polymer-salt intercalation into nanometric channels of organo clay films.

as a function of applied load. The data so obtained for each PNC electrolyte films has been used to evaluate stress and the corresponding strain produced in the material under the experimental condition.

RESULTS AND DISCUSSION

XRD analysis

The XRD pattern of the PNC films under investigation is shown in Figure 1(a,b). The pattern shown in Figure 1(a) comprises of characteristic PAN peak observed at 2θ is ~ 14.1° and 22.5°. The presences of these peaks are attributed to the crystalline component of the host polymer (PAN), which has hexagonal crystal structure.[11] The miller indices of the PAN peaks are [010] and [300] as shown in the XRD pattern of the PS film. It does not contain any XRD peak of the salt ($LiCF_3SO_3$) suggesting complete salt dissolution in the polymer matrix by way of complexation. The addition of organomodified montmorillonite clay in increasing order of concentration into the PS matrix is indicated by the appearance of additional peaks in the XRD pattern [Figs. 1(a),(ii–viii)]. The intensity of this new peak appears to increase with rise in clay concentration. The peak may be attributed to clay component confirming thereby composite nature of the sample films.

To observe the effect of clay concentration on changes occurring in the structural phase properties of the polymer (PAN) host in the PNC films, a systematic analysis of both polymer host [010] and organomodified clay [001] observed at 2θ is ~ 14.1° [12] and 5.8° [13] respectively has been carried out. The PAN peak profile in PNC film appears to change as observed in terms of relative change in polymer main peak, peak intensity, d-spacing, and polymer interchain separation given in Table I. The intensity of PAN peak in the PNC films has been observed to decrease with increase in clay concentration except at very low clay loading. This result indicates a relative increase in the amorphous phase fraction of the host polymer in PNC films. In addition, the d-spacing and polymer interchain spacing has been calculated using the relation;

$$2d\,\mathrm{Sin}\theta = n\lambda \tag{2}$$

and

$$R = \frac{5}{8}\left(\frac{n\lambda}{Sin\theta}\right) \; where\; n = 1, 2, 3 \tag{3}$$

valid for noncrystalline polymers. The estimated values suggest minor changes in the PNC films in comparison to that of the PS.

However, drastic changes in the d_{001} peak profile of the clay observed at 2θ ~ 5.8° has been noticed to occur. Figure 1(b) shows marked changes in the pattern of clay in terms of peak shift toward low angle side, increase in d-spacing, reinforced peak intensity up to 15 wt % and enhancement in the clay gallery width in the PNC films when compared with pure clay XRD data. The changes are recorded in the

TABLE I
Changes in the Structural Parameters of the Host Polymer (PAN) Evaluated from the XRD Peak [010] Profile of the Pan in the PNC Films [$(PAN)_8LiCF_3SO_3$ + *x* wt % DMMT]

Clay Conc. (wt %)	I_{comp} / I_{ps}	d-Spacing (Å)	Polymer interchain spacing (R) (Å)
$x = 0$	100	6.2	7.6
$x = 1$	116	6.3	7.7
$x = 2$	105	6.2	7.6
$x = 5$	66	6.3	7.7
$x = 7.5$	60	6.2	7.6
$x = 10$	63	6.2	7.6
$x = 15$	57	6.1	7.4
$x = 20$	84	6.1	7.4

TABLE II
Intercalation of Polymer-salt Complex nto the Nanometric Clay Galleries of Organomodified Clay in the PNC Films Based on $(PAN)_8LiCF_3SO_3$ + x wt % DMMT

Clay Conc. (%)	Pos.(2θ)	d-Spacing(Å)	Clay Gallery width(Å)
Clay	5.8	15.1	5.5
$x = 2$	5.4	16.4	6.8
$x = 5$	4.5	19.3	9.7
$x = 7.5$	4.5	19.2	9.6
$x = 10$	4.5	19.5	9.9
$x = 15$	4.5	19.2	9.6
$x = 20$	4.5	19.3	9.7

Table II. Substantial enhancement in the clay gallery width has occurred up to ~ 5 wt % clay concentration in PNC films and remains almost constant thereafter. The enhancement in the clay channel width on incorporating clay into PS matrix provides a convincing evidence of the intercalation of cation coordinated polymer chain into the nanometric clay galleries. The intercalation effect appears to be significantly stable for clay concentration x ≥ 10 wt %. An indication of this feasibility is also confirmed by observed changes in the intensity profile of the PNC films. The XRD result clearly provides evidence of a very strong interaction between PS complex and clay in the PNC films.

Transmission electron microscope (TEM) analysis

TEM analysis has been performed to observe the surface property and morphological features of the PNC films. Figure 2(a–f) depicts TEM micrographs and selected area electron diffraction (SAED) pattern of PNC films with different clay concentration. The typical morphology of the clay free PS complex matrix [Fig.(2a)], comprises of PS complex phase, whereas the PNC films with 2 wt % clay concentration [Fig.(2b)] shows the appearance of DMMT clay layers clearly. It also suggests the presence of exfoliation of the PS matrix in the PNC at low clay loading. At low clay loading there have to be presence of individual clay platelets dispersed homogeneously in PS matrix indicates that some exfoliation has occurred in PNC films. The dark slices present in the image represent the exfoliated PNC film, which is also confirmed in the XRD spectrum shown in the Figure 1(b).[14] However, with increase in the clay concentration, the scenario changes completely. A representative TEM graph for higher clay concentration (15 wt % clay) clearly depicts the presence of regions indicated by the presence of well-defined stacks representing clay channels with PS [Fig. 2(c)]. At higher clay loading, a number of intercalated tactoids are observed to be dispersed into the PS complex matrix.[15] The SAED pattern confirms that the crystalline nature of the PNC films has improved on nanocomposite formation and the effect appears to be stronger with increasing clay concentration in the PNC films [Fig. 2 (d–f)].

Complex impedance analysis

Figure 3 shows complex impedance spectrum (CIS) pattern of PAN based solid polymer films for 5 wt % clay concentrations and without clay at room temperature and 80°C. The CIS pattern comprises of a response typical to a small high frequency arc followed by a steep spike in the low frequency region.[16] The intercept of the spike on real axis gives an estimate of bulk resistance (R_b) of the sample. The experimental impedance response, when fitted using nonlinear least squares (NLS) model by means of a computer program (ZSimpWin), agrees well with the theoretical plot (Solid lines). An electrical equivalent circuit model of the sample impedance

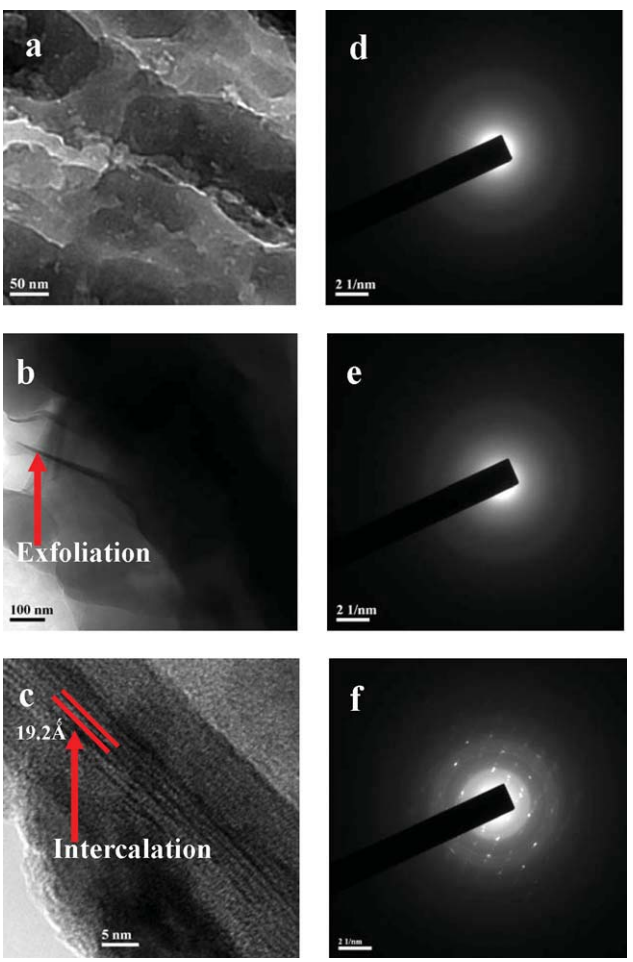

Figure 2 TEM and selected area electron diffraction (SAED) pattern of PNC films at organomodified clay concentration (x = 0, 2, and 15%). [Color figure can be viewed in the online issue, which is available at www.interscience.wiley.com.]

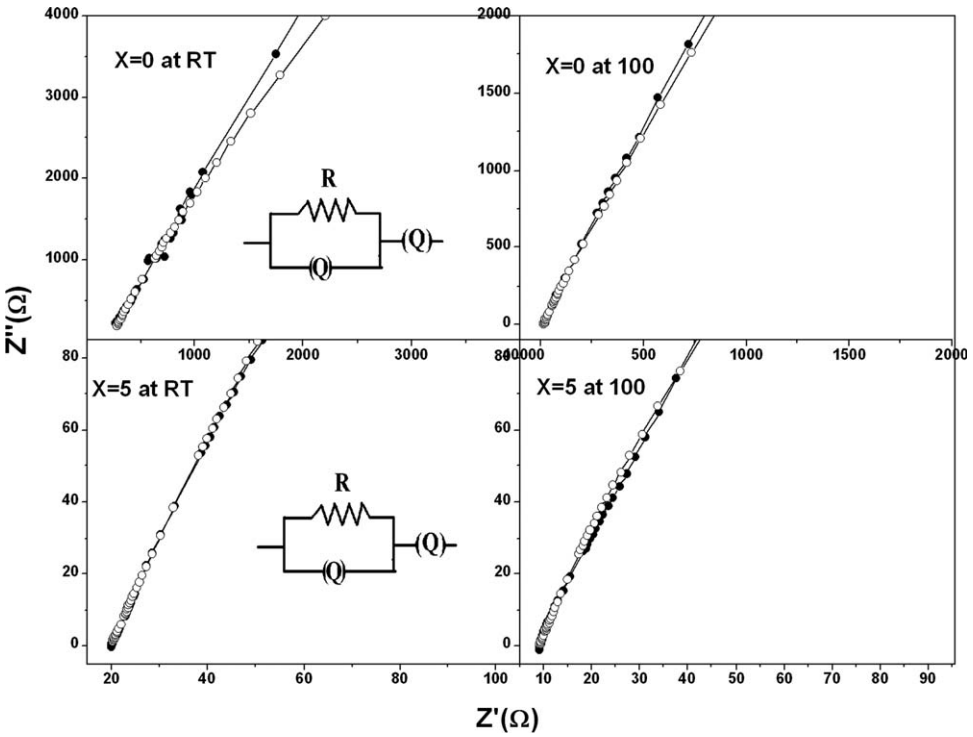

Figure 3 Nyquist plot of PNC films at room temperature and 80°C based on $(PAN)_8LiCF_3SO_3$ + *x* wt % DMMT.

response appears to be consistent with a fit comprising of parallel combination of resistance (*R*) and the constant phase element (cpe) connected in series with another constant phase element (cpe). The presence of a constant phase element (cpe) in the material sample is a testimony of its multiphase character comprising of microstructure having both crystalline, amorphous and an intermingling of the two phases in the PS complex (PS) films. The constant phase element (cpe) is generally used in place of pure capacitor in real systems and its impedance is expressed as; $Z_{CPE} = \frac{1}{Q_0(j\omega)^n}$ where Q_0 and n are fitting parameters, $n = 0$ for pure resistor, $n = 1$ for pure capacitor, and $n = 0.5$ having the both resistive and capacitive component.

The parameters given in the Tables III and IV of the manuscript are just to provide evidence for change in the sample electrical response with change in clay concentration in the PNC films. The estimated value of *Q* and its exponent for "cpe" components of the electrical equivalent circuit model for PNC films with different clay concentration at RT and 80°C are presented in the Tables III and IV. The effect of clay addition into the $(PAN)_8LiCF_3SO_3$ matrix appears to modulate the electrical behavior of the PNC films with increase in the clay concentration.

This is reflected clearly, in the CIS pattern (Nyquist plot) on clay addition (say 5 wt %) in comparison with that of the PS film without clay,

TABLE III
Typical Values of the Electrical Parameters Obtained from Nonlinear Least Squares (NLS) Fit of the Impedance Spectrum of the PNC Films [$(PAN)_8LiCF_3SO_3$ + *x* wt % DMMT] at Room Temperature

		Impedance Parameters					
		Bulk data		Interface data			
Clay conc. (%)	Rb (Ω)	Q_1	n_1	Q_2	n_2	σ_{dc} at RT	C_{dl} (μF)
$x = 0$	272	3.0×10^{-6}	0.28	1.5×10^{-7}	0.78	2.4×10^{-4}	18
$x = 1$	75.0	4.8×10^{-6}	0.30	3.2×10^{-7}	0.80	1.2×10^{-3}	45
$x = 2$	6.8	1.9×10^{-5}	0.48	1.7×10^{-5}	0.83	8.4×10^{-3}	530
$x = 5$	7.8	2.4×10^{-5}	0.46	7.5×10^{-6}	0.82	6.7×10^{-3}	212
$x = 7.5$	9.9	9.2×10^{-5}	0.51	2.4×10^{-6}	0.90	6.8×10^{-3}	53
$x = 10$	9.1	4.0×10^{-5}	0.40	2.4×10^{-5}	0.51	5.9×10^{-3}	80
$x = 15$	12.4	1.8×10^{-5}	0.39	1.8×10^{-5}	0.76	4.7×10^{-3}	265
$x = 20$	12.7	9.1×10^{-5}	0.45	2.5×10^{-5}	0.73	3.7×10^{-3}	289

TABLE IV
Typical Values of the Electrical Parameters Obtained from Nonlinear Least Squares (NLS) Fit of the Impedance Spectrum of the PNC Films [$(PAN)_8LiCF_3SO_3$ + x wt % DMMT] at 80°C

		Impedance Parameters					
		Bulk data		Interface data			
Clay conc. (%)	Rb(Ω)	Q_1	n_1	Q_2	n_2	σ_{dc} at 80°C	C_{dl} (μF)
$x = 0$	24.8	4×10^{-6}	0.31	2.3×10^{-6}	0.72	3.8×10^{-3}	47
$x = 1$	30.8	9.8×10^{-6}	0.56	8.6×10^{-6}	0.77	4.9×10^{-3}	227
$x = 2$	28.0	1.1×10^{-6}	0.77	7.6×10^{-5}	0.80	2.5×10^{-2}	227
$x = 5$	9.2	3.9×10^{-6}	0.48	3.9×10^{-5}	0.72	1.4×10^{-2}	531
$x = 7.5$	11.5	7.5×10^{-6}	0.49	4.7×10^{-4}	0.86	1.9×10^{-2}	227
$x = 10$	10.6	3.7×10^{-5}	0.49	6.6×10^{-5}	0.85	1.5×10^{-2}	265
$x = 15$	8.2	2×10^{-5}	0.49	$4.3 \times 3\ 10^{-5}$	0.85	6.7×10^{-3}	159
$x = 20$	14.0	9.6×10^{-5}	0.48	3.6×10^{-5}	0.88	6.7×10^{-3}	159

indicated by a relatively steeper spike in the former. A NLS fitting of the experimental data shows good agreement with the corresponding theoretical pattern suggesting validity and accuracy of the experimental results. The model of electrical equivalent circuit remains identical in pattern for the PNC and PS films with essential difference in the values of bulk resistance (R_b), constant phase elements Q_1 and Q_2 and their exponent's n_1 and n_2, respectively. A lowering in the value of "n" indicates enhancement in the phase inhomogeneity of the PNC film on PS intercalation into the clay channels. The CIS pattern remains almost identical even at 80°C with essential difference in the substantial lowering of the value of bulk resistance (R_b) and almost identical changes in the value of constant phase element components and their exponents. The value of "Q" and "n" for various composition of $0 \leq x \leq 20$ of the PNC at RT and 80°C have been recorded in the Tables III and IV for comparison. It clearly indicates the presence of double layer capacitance (electrode polarization effect) at the electrode-electrolyte interface. This inference also seems to be reasonable and consistent with the estimated value of C_{dl} (double layer capacitance), which is of the order of μF for the PNC film in sharp contrast to PS film. This observation appears to be consistent with the prevailing concepts in the case of fast ion conducting solids.

Ionic transport and conduction properties

Ion transport property has been studied in two steps described as follows:

Separation of ion and electronic contribution

Figure 4 shows the typical variation of polarization current as a function of time for both the PS and PNC films of different clay concentration recorded at room temperature. The pattern of variation shows a very high initial total current (I_t) followed by a sharp drop in its value with the passage of time. The current ultimately attains a saturation value and remains invariant as a function of time. The initial high current is attributed to the contribution from both the ions and the electron in the sample matrix whereas the final saturation current is attributed to the contribution of electronic mobility. It is known as residual electronic current (I_e). The experimental pattern of variation (Fig. 4) follows almost identical trend for both the PS and PNC films. The estimated value of the ionic transport number (t_{ion}) using experimental data of I_t and I_e in accordance with the eq. (1) are given in the Table V. The transport number values clearly indicate that the PNC samples are predominantly ionic conductor with ion transport number (t_{ion}) close to unity.

The ion transport results have also been used to estimate ionic and electronic contributions to the

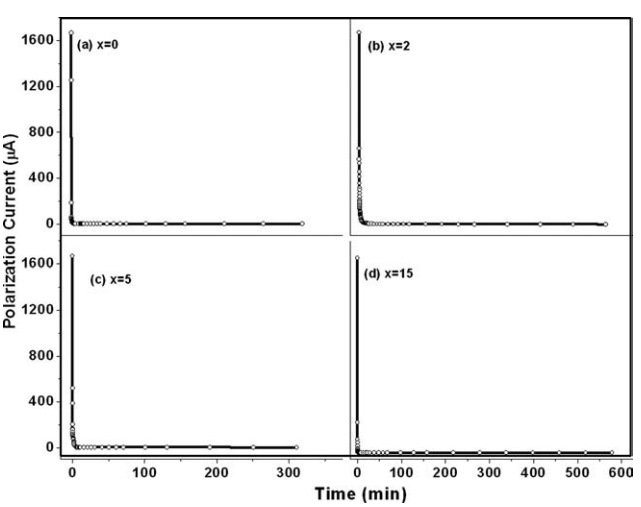

Figure 4 Variation of polarization current as a function of time for PNC films [$(PAN)_8LiCF_3SO_3$+ x wt % DMMT] with various clay concentration.

TABLE V
Ionic Transport Number and Electrical Conductivity Because of Electronic and Ionic Contributions for Various Clay Concentrations in the PNC Films Based on $(PAN)_8LiCF_3SO_3$ + x wt % DMMT

NaMMT Clay x (%)	Transport No. (%)	Ionic Conductivity (S cm^{-1})	Electronic Conductivity (S cm^{-1})
$x = 0$	99.9	2.39×10^{-4}	3.0×10^{-7}
$x = 2$	99.7	8.37×10^{-3}	7.2×10^{-6}
$x = 5$	99.6	6.67×10^{-3}	26.8×10^{-6}
$x = 15$	99.8	4.69×10^{-3}	9.4×10^{-6}

electrical conductivity in accordance with the equation $\sigma_{ion} = \sigma_{dc} \times (t_{ion})$ and $\sigma_e = 1 - \sigma_{ion}$. The calculated conductivity values are given in the Table V. The ionic conductivity value is $\sim 10^{-3}$ S cm^{-1} almost for all the PNC films, which is well in the desirable limit and at par with the liquid electrolytes. However, electronic conductivity value $\sim 10^{-6}$ S cm^{-1} may be considered to be in the ideal limit of the suitability for ionic device applications.

Separation of anion and cation contribution in the overall electrical transport

To see the actual contribution of cations to the electrical transport properties of PNC films, we have evaluated the Li^+ ion transport property using a combined dc polarization / ac impedance measurement technique[10] proposed by Vincent and coworkers. The formula used for evaluating the cation transport number is:

$$t_{Li} = \left(\frac{I_S(V - I_o R_o)}{I_o(V - I_S R_S)} \right) \quad (4)$$

where V is the applied dc voltage for sample polarization, I_o and I_s are the currents before and after polarization whereas R_o and R_s are the initial and steady-state resistance of the passivating layers. Figure 5(a,b) gives the estimation of steady-state resistance before and after polarization, respectively. The impedance measurement on the cell using nonblocking electrode was performed before and after cell polarization at a relatively smaller dc field (20 mV) applied across it. The dc polarization was allowed for a considerably larger time (12 h). The impedance response and variation of polarization current vs. applied dc field is shown in Figure 5(a–c). The experimentally measured values of sample electrical response parameters as per the eq. (4) are; dc voltage $\sim$ 20 mV, $R_o = 103\ \Omega$, $I_o = 30$ nA, $R_s = 4330\ \Omega$, and $I_s = 20$ nA. Using these values in eq. (4), the estimated value of cationic transport number (t_{Li}^+) for PAN+$LiCF_3SO_3$+15 wt % DMMT film is $\sim$ 67%. It is higher in comparison to a number of polymer (PAN)-salt complex such as; PAN-$LiClO_4$ ($\sim$ 60%), PAN-$LiAsF_6$ ($\sim$ 40%) and PAN-$LiN(CF_3SO_2)_2$ ($\sim$ 60%).[17] A comparison of the cation transport values suggests a clear enhancement in t_{Li+} on intercalation of PAN + $LiCF_3SO_3$ complex into the nanometric clay galleries of the organomodified clay.

STABILITY PROPERTIES

Voltage stability

The optimum limit of voltage stability (also known as electrochemical potential window or working voltage of the intercalated polymer-clay nanocomposite films) has been studied by measurements of the residual electronic current as a function of the applied voltages. Typical I–V characteristic curves for PS and PNC films of different clay concentration are shown in the Figure 6(a–d). It indicates a gradual increase in the magnitude of current with rise in the applied voltage across the cells. As the voltage increases beyond a certain threshold limit, an abrupt enhancement in current occurs and current keeps on rising as if the applied dc bias losses control on current flow across the cell. This behavior appears to be distinctly different for the PS complex film and intercalated PNC films. The result provides a clear indication of substantial enhancement in the voltage stability limit of PNC films when compared with PS film without clay. Of course, the voltage stability enhancement appears to be a function of clay concentrations evident from the results. The stability limit has been estimated from intercept of the tangent to the suddenly rising current on voltage axis. These values for the selected PNC films with 2 wt % and 5 wt % clay concentration are given in the Figure 6 and have been compared with the stability window of clay free PS film. A comparison indicates substantial improvement in the voltage stability window in the PNC films with the highest stability value of $\sim$ 5.6 V for the sample with 5 wt % clay concentration. However, it is important to mention at this stage that limit of voltage stability again starts falling down at clay concentration $\geq$15 wt %. The voltage stability achieved for PAN based solid PNC film with 5 wt % clay appears to be at par with the voltage stability window of the conventional liquid electrolytes. Further this value for PAN based PNC is perhaps the highest among polymer based solid ionic conductors. Before this report, the highest value of voltage stability reported in literature is $\sim$ 5 V for ion conducting polymeric system; composite polymer electrolyte (3.75 V, 4.75 V),[18,19] solid polymer electrolyte (4.7 V),[20] and gel polymer electrolyte (5 V).[17,21]

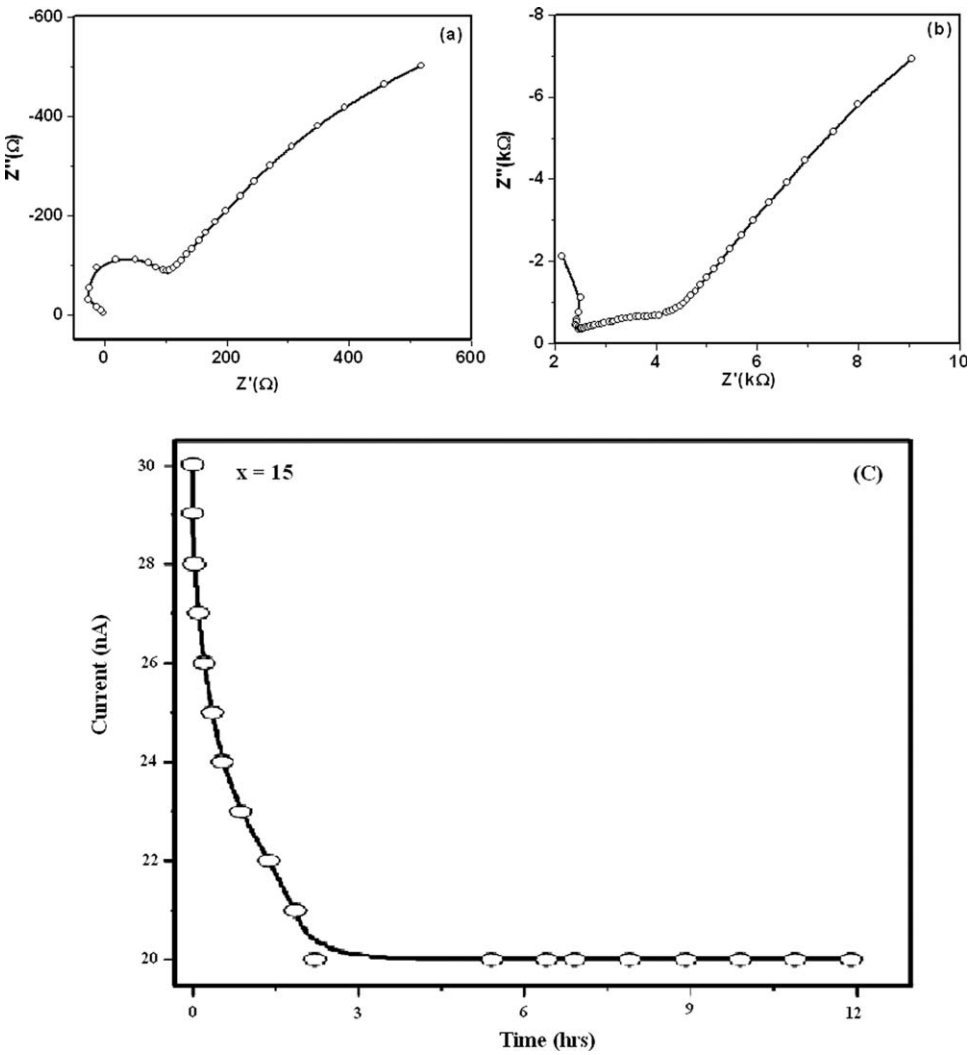

Figure 5 Electrochemical impedance spectrum (EIS) of the cell (a) before polarization, (b) after polarization, and (c) variation of polarization current with time at an applied dc field (20 mV).

Thermal stability

The effect of clay concentration on thermal stability property of the PNC films has been investigated by TGA. The TGA pattern of the films with the various clay concentrations is shown in the Figure 7. It shows three clear regions of changes suggesting three distinct thermal transitions marked as I, II, and III in the Figure 7. It may be indicative of different physical processes occurring with the system. The first region (I) in the thermogram indicates a progressive mass loss that continues up to 250°C followed by a kink at 270–280°C. It may be attributed to the stabilization of polymer backbone via formation of ring because of cyclo cross-linking among the adjacent —CN groups. The second region (II) in the TGA pattern occurring in the temperature range 280–350°C represents the zone where the rate of mass loss is relatively steady with a change in slope. It may be related to chain flexibility of the polymer backbone near its melting temperature (317°C).

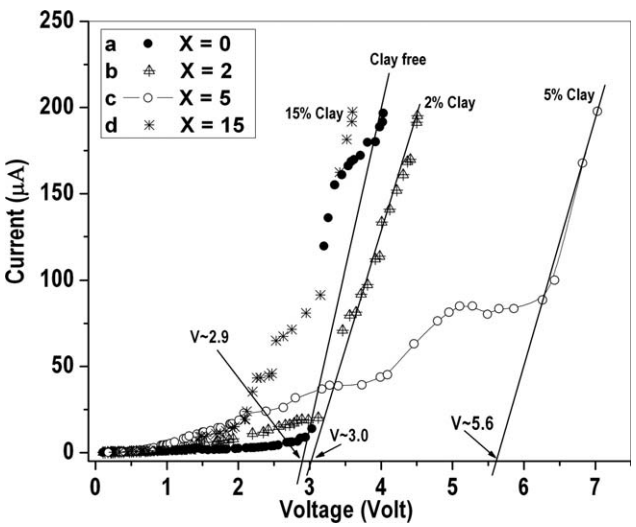

Figure 6 Variation of residual electronic current as a function of applied dc voltage (I–V characteristics) of PNC films [$(PAN)_8LiCF_3SO_3$ + x wt % DMMT] with various clay concentration.

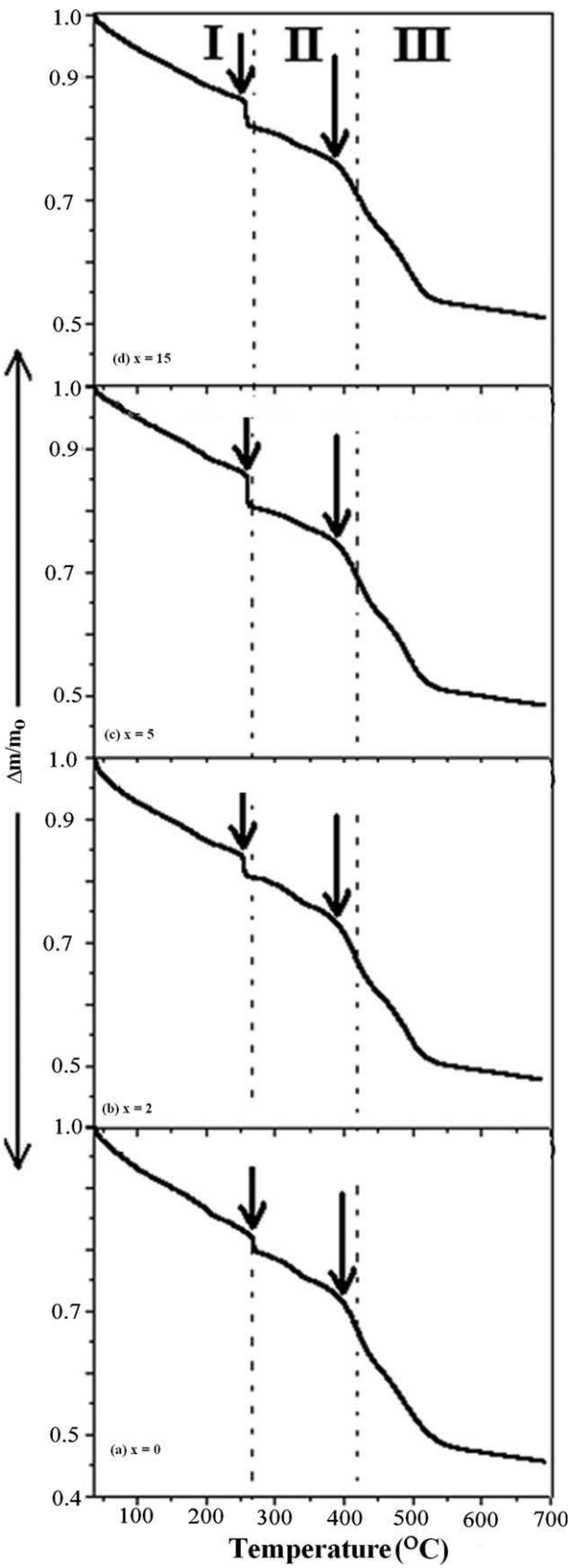

Figure 7 Thermogravimetric analysis (TGA) curves of PNC films [$(PAN)_8LiCF_3SO_3 + x$ wt % DMMT] for various clay concentrations.

However, the possibility of cyclocrosslinking reaction and evolution of volatile component from PAN backbone cannot be ruled out. In the region (III) occurring at temperatures above 350°C, there is steep fall in mass. This may be because of thermo-oxidative degradation and polymer chain scission. Although, apparently, thermal stability appears to be lowered with increase in clay concentration by 10 to 15°C, the thermal stability up to a temperature range of the order of 250°C is quite acceptable for energy storage device application. The inference appears to be consistent with a few previous reports in literature.[14,22,23]

In addition, the drastic enhancement of voltage stability on nanocomposite formation adds sufficient value to the experimental limits of thermal stability indicated by TGA analysis.

Mechanical stability

The mechanical properties of thin PNC films have been observed in terms of their tensile strength (TS) and maximum percentage elongation (EL) at break. The result of mechanical measurements has been expressed in the form of stress–strain diagram shown in the Figure 8(a–d). It provides valuable information of the material mechanical properties such as the nature of deformation under an external load, tensile strength (TS), etc. A comparison of these parameters of the clay based nanocomposite films with that of the pure PS complex is expected to provide significant information for justification of nanocomposite formation.

A typical representative stress-strain diagram for clay free sample i.e. $(PAN)_8LiCF_3SO_3$ is shown in the Figure 8(a). It shows a linear relationship between stress and strain up to a limiting stress of 6.7 MPa in strict agreement with ideal elastic system obeying Hooke's law. Beyond this, a nonlinear variation followed by a kink is observed. Finally, the mechanical breakdown of the sample occurs at a stress of $\sim$ 5 MPa with percentage elongation at break being 100%. We attribute this change possibly to elastic fatigue. Although such a behavior against an applied load has already been reported[24,25] previously without any explanation. The estimated value of elastic constant (Young modulus) from the stress-strain plot is 426 MPa for the clay free PS film.

A clear change in mechanical behavior has been observed in the PNC films even at a lower clay loading ($\sim$ 2 wt %). The variation in the stress-strain plot shows typical linear pattern [Fig. 8(b)] without any signal for nonlinearity even at higher applied load unlike that of the PS film. This change itself indicates significant improvement in the mechanical properties. This is also confirmed by substantial enhancement in the value of TS ($\sim$ 16 MPa) and

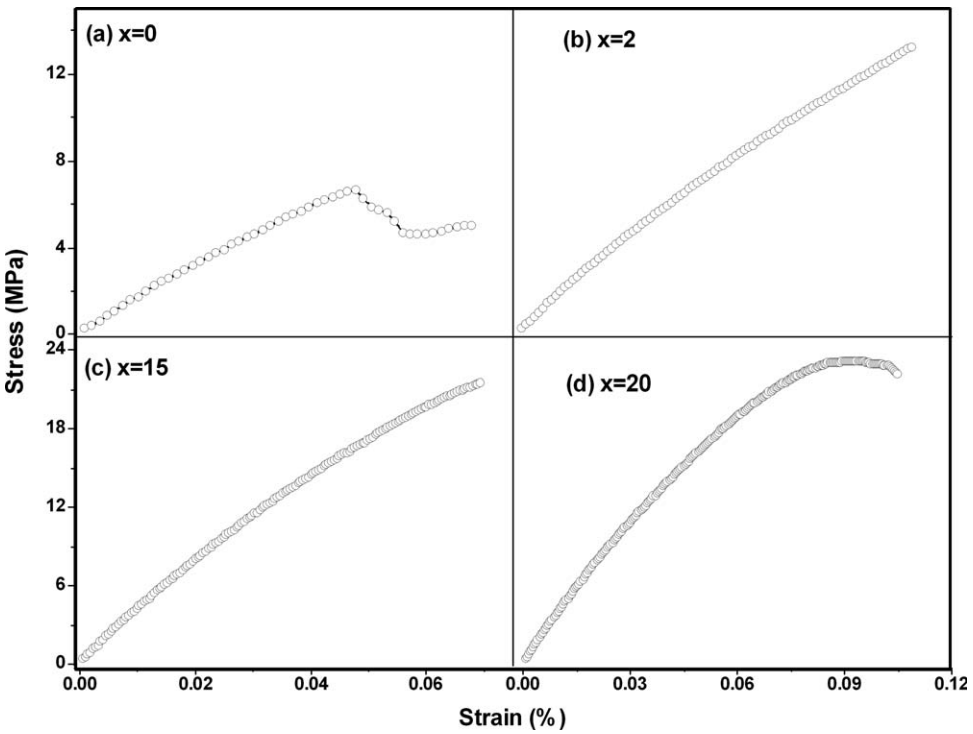

Figure 8 Stress-strain diagram of PNC films based on $(PAN)_8LiCF_3SO_3 + x$ wt % DMMT.

elongation (200%) that amounts to a two fold increase in the mechanical properties.

On further increase in the clay loading ($\sim$ 15 wt %), a clear change in the tensile strength (TS), maximum percentage elongation (EL) at break and the modulus of elasticity has been noticed in the stress-strain diagram of the PNC films. Finally, at 20 wt % clay concentration, the linear relationship in stress-strain diagram undergoes modification with two distinct regions that can be identified as the regions of elastic and plastic deformation before the sample breakdown takes place. The estimated value of the tensile strength in the 20 wt % clay is about $\sim$ 25 MPa with the maximum percentage elongation being $\sim$ 400%. The young modulus value works out to be $\sim$ 308 MPa.

A relative comparison of the effect of clay loading on changes in the mechanical properties is described in terms of the degree of variation in the TS shown in the Figure 9. It shows the variation in tensile strength (TS_{max}) against modified clay concentration. From figure it clearly indicates that addition of the clay causes substantial enhancement in the mechanical stability to the tune of 3–4 times when compared with the mechanical stability of pure PS complex sample. It may possibly be attributed to the role of clay as a supporting matrix for reinforcing the strength via an improved molecular interaction within the polymer matrix. The stress-strain plot (Fig. 8) has also provided an estimate of young modulus for PNC films with different clay concentration. Typical representative results are shown in the Table VI for comparison. The results indicate a lowering in the young modulus of PNC films with increasing clay concentration. This result may be related to a possible flexibility in the polymer matrix backbone and it may be linked with shock absorbing ability of the PNC films under stress. The onset of this behavior occurs even at very low clay concentration of 2 wt % as evident from the table and it attains

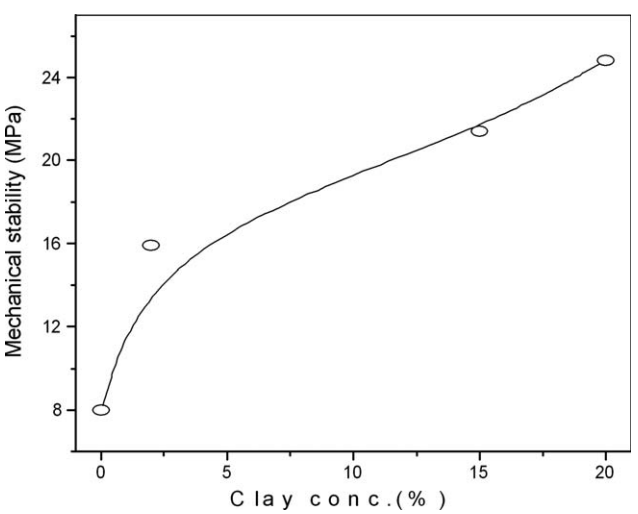

Figure 9 Typical variation of tensile strength (TSmax) as a function of clay concentration.

TABLE VI
Typical Representative Mechanical Properties (Tensile Strength, Young Modulus, and Relative Change in Elongation at Break) of PNC Films Based on $(PAN)_8LiCF_3SO_3 + x$ wt % DMMT

Clay Conc.(%)	Young Modulus(Y)	TS (MPa)	ΔEL (%)
0	426	5	100
2	377	16	200
15	307	20	300
20	307	25	400

saturation limit at 15–20 wt % clay concentration. The overall impact is an improvement in the mechanical properties on nanocomposite formation.

SUMMARY AND CONCLUSIONS

A new series of intercalation type PNC film based on $(PAN)_8LiCF_3SO_3 + x$ wt % DMMT has been prepared and characterized for its structural, morphological, electrical, thermal, mechanical, and transport properties. XRD results confirm composite formation and provide evidence for strong interaction of PS matrix with organomodified clay. Quantative analysis of XRD data clearly suggests the intercalation of PS matrix into nanometric clay channels. Such a possibility is strongly corroborated by transmission electron microscopy (TEM) results. CIS results provide evidence of bulk conduction as the major electrical transport process in both the PS and PNC films. A modeling of the sample electrical behavior suggests that both the PS and PNC films behave electrically as an equivalent electric circuit comprising of parallel combination of resistance with constant phase element (cpe) connected in series with another constant phase element (cpe). The presence of second constant phase element is consistent with the evidence of charge accumulation at the electrode-electrolyte interface. Ion transport number ($\sim$ 0.99) results indicate the PNC films to be predominantly ionic whereas the cationic transport number is substantially higher ($t_{Li}{}^{+} \sim$ 0.67). Large enhancement in voltage stability (5.6 V) and mechanical stability ($\sim$ 25 MPa) have been recorded on nanocomposite formation. Thermal stability ($\sim$ 250°C) of the PNC films appears to be quite acceptable for device application. The optimized combination of the PNC film may be expected to serve the dual purpose of electrolyte and separator in energy storage device such as the lithium polymer batteries and supercapacitors etc.

One of the authors (A. L. Sharma) gratefully acknowledges the financial support received from Council of Scientific and Industrial Research (CSIR), Govt. of India, New Delhi for carrying out research at the Department of Physics and Meteorology, Indian Institute of Technology (IIT) Kharagpur-721302, India.

References

1. Perera, K.; Disanayake, M. A. K. L.; Bandaranayake, P. W. S. K. Mater Res Bull 2004, 39, 1745.
2. Appetecchi, G. B.; Croce, F.; Scrosati, B. Electrochim Acta 1995, 40, 591.
3. Sharma, A. L.; Shukla, N.; Thakur, A. K. J Polym Science: Part B: Polym Phys 2008, 46, 2577.
4. Tsutsumi, H.; Kitagawa, T. Solid State Ionics 2006, 177, 2683.
5. Perera, K.; Dissanayake, M. A. K. L.; Bandaranayake, P. W. S. K. Electrochim Acta 2000, 45, 1361.
6. Chang, C. C.; Hou, S. S. Eur Polym J 2008, 44, 1337.
7. Hocine, N. A.; Mederic, P.; Aubry, T. Polym test 2008, 27, 330.
8. Forsyth, M.; Farlane, D. R. M.; Hill, A. J. Electrochim Acta 2000, 45, 1243.
9. Nam, J. D.; Hwang, S. D.; Choi, H. R.; Lee, J. H.; Kim, K. J.; Heo, S. Smart Mater Struct 2005, 14, 87.
10. Evans, J.; Vincent, C. A.; Bruce, P. G. Polymer 1987, 28, 2324.
11. Joint Committee of Powder Diffraction Standard—International Center for Diffraction Data (JCPDS-ICDD) 48–2119.
12. Boguslavsky, L.; Baruch, S.; Margel, S. J Colloid Interface Sci 2005, 289, 71.
13. Kim, S.; Park, S. J. Solid State Ionics 2007, 178, 973.
14. Yu, T.; Lin, J.; Xu, J.; Chen, T.; Lin, S.; Tian, X. Compos Sci Technol 2007, 67, 3219.
15. Kurian, M.; Galvin, M. E.; Trapa, P. E.; Sadoway, D. R.; Mayes, A. M. Electrochim Acta 2005, 50, 2125.
16. Thakur, A. K.; Pradhan, D. K.; Samantaray, B. K.; Choudhary, R. N. P. J Power Sources 2006, 159, 272.
17. Croce, F.; Gerace, F.; Dautzemberg, G.; Passerini, S.; Appetecchi, G. B.; Scrosati, B. Electrochim Acta 1994, 39, 2187.
18. Leo, C. J.; Thakur, A. K.; Rao, G. V. S.; Chowdari, B. V. R. J Power Sources 2003, 115, 295.
19. Yang, Y. W. C.; Chen, Y. T.; Chen, H. C.; Lin, W. T.; Tsai, C. H. Polymer 2009, 50, 2856.
20. Park, J. W.; Jeong, E. D.; Won, M. S.; Shim, Y. B. J Power Sources 2006, 160, 674.
21. Capuano, F.; Croce, F.; Scrosati, B. J Electrochem Soc 1991, 138, 1918.
22. Mehr, M. J. Z.; Pourjavadi, A.; Sadeghi, M. Iranian Polym J 2005, 14, 131.
23. Mei, M. A. J.; Yuan, S. X.; Rui, W. Q. http://www.paper.edu.cn/en/downloadpaper.php?serial_number=200511-12&type=1.
24. Fiorellia, J.; Diasb, A. A. Mater Res 2003, 6, 193.
25. Buchanan, A. H. J Struct Eng 1990, 116, 1213.